

Quantum circuit for toric code state preparation via graph states

Pengcheng Liao and David L. Feder*

*Institute for Quantum Science and Technology, and Department of Physics and Astronomy,
University of Calgary, Calgary, Alberta, Canada T2N 1N4*

Given the wide applicability of topological states for fault-tolerant quantum computation, an important outstanding question is how to generate these states within the quantum circuit model, and if it is possible to do so efficiently. In this work, toric code states on the torus are mapped to an equivalent graph state under local Clifford operations. The graph is composed of only two subgraphs, both of which can be generated in log depth, assuming geometrically non-local gates. Including ancillae and measurements, the circuit depth can be reduced to a constant at the cost of increasing the circuit width. Among many insights, the toric code graph structure reveals a close connection between repetition and topological codes. Due to their local equivalence to the toric code, all two-dimensional translationally invariant topological stabilizer codes are therefore efficiently preparable on a quantum circuit. The results provide a new graph-theoretic framework for the development of novel topological error correction codes, beyond geometrical considerations.

I. INTRODUCTION

Since the idea of topological quantum computation was first introduced by Kitaev in the form of the celebrated toric code [1–3], interest in finding ways to generate topological states and implement topological operations has remained strong [4–6], due to the potential for the implementation of fault tolerant quantum gates with extremely high error thresholds [7]. In condensed matter physics, topologically ordered states are usually framed as the degenerate ground states of a specially chosen gapped local Hamiltonian [8–15]. In the quantum information community, topological models are framed in terms of stabilizers, which underpin the framework of quantum error correction [16]; for example, the toric code states are the four-fold degenerate eigenstates of a ‘Hamiltonian’ consisting of the negative sum of $N - 2$ toric-code stabilizer generators, where N is the number of physical qubits. Fault-tolerant operations can then be implemented by manipulating the constituent qubits to effect braiding operations, which effects operations on the two qubits encoded in the degenerate ground states. The toric code is the most well-studied topological model, not only because of its apparent simplicity, but also because all two-dimensional translationally invariant topological codes (so-called surface or planar codes, depending on the boundary conditions) are equivalent to it [17].

Generating topological states as the ground states of an effective Hamiltonian is not possible within the quantum circuit model for quantum computation, which usually consists of a set of (dissipationless) unitary gates acting on an unentangled quantum input state. For practical reasons, it is therefore important to understand the complexity of preparing topological states via a quantum circuit. The complexity in this context is taken to mean the circuit depth, the scaling in number of non-parallelizable quantum gates with the size of the input.

Furthermore Chen et al. [18] have shown that quantum states are topologically trivial if they can be generated by a constant-depth quantum circuit; thus the circuit depth for quantum state preparation can potentially provide insights into the classification of topological order and for the detection of topological phase transitions [19].

Using Lieb-Robinson bounds for Hamiltonian evolution, Bravyi et al. [20] proved that the time complexity lower bound to create a topological state from a trivial one is proportional to the size of system. This lower bound is confirmed to be tight for the ground state generation of toric code through adiabatic evolution [21]. The equivalence of adiabatic evolution and the quantum circuit model for state generation [22] then implies that the lower bound to generate topological states using a quantum circuit composed of geometrically local gates (i.e. gates only between qubits that are nearest-neighbors to one another) is proportional to the system size [23, 24]. Thus the ground state of the 2D toric code of $N = 2L^2$ qubits positioned on both horizontal and vertical edges of an L by L array requires a quantum circuit of depth at least $\Omega(\sqrt{N})$.

Given that there are a variety of schemes to implement non-local gates (usually via an additional classical communication overhead) [25–31], culminating in an experimental demonstration for a five-qubit system [32], it is of both practical and theoretical value to determine the complexity of topological state preparation relaxing the geometrical local-gate assumption. Recently, Aharonov [33] proved that the lower bound for generating (topological-trivial) cube states is $\Omega(\log N)$ in this setting, and the same lower bound for the generation of toric code states is obtained as a corollary; moreover, this work contains a proof (attributed to Bravyi) that topological states cannot be generated by a constant-depth circuit, echoing the result by Chen et al. [18]. The tightness of the lower bound can also be inferred from Ref. [34]. That said, an explicit construction of a log-depth quantum circuit remains unknown; obtaining this is one of the main results of the present work. Intriguingly, the depth can in fact be reduced to a constant with the inclusion of an-

* Corresponding author: dfeder@ucalgary.ca

cillae and projective measurements, though at the cost of increasing the circuit width relative to the size of the input.

We approach this problem by mapping the toric code state on a two-torus to a quantum graph state, making use of the fact that every stabilizer state is equivalent to a graph state under local Clifford (LC) gates [35, 36]. The main motivation for performing this transformation is that the quantum circuit for the preparation of a graph state can be obtained directly from the graph itself; all qubits (graph vertices) are initially prepared in the $+1$ eigenstate of the Pauli X operator, and controlled-phase (CZ) gates are applied between qubits whenever the vertices share an edge.

The degenerate toric code has two fewer stabilizer generators than is the case for graph states. In order to effect the map, one may supplement the generators with two closed ‘string’ operators; these consist of contiguous strings of X and Z gates that encircle the torus, which commute with all toric-code stabilizer generators and with one other. In this way, one can obtain the graph state that is LC-equivalent to any of the ground states of the 2D toric code, depending on the orientation of the string operators; these states are denoted as *toric graph states* in this work. These kinds of string operators correspond to the logical X and Z gates in the toric code, and can therefore map the target toric graph state to any other after the state preparation. Furthermore, as the strings have length $L \sim \sqrt{N}$, the toric code distance is macroscopic as it scales with the number of physical qubits. The macroscopic code distance is a characteristic of the toric code and is a suitably proxy for the existence of topological order.

We find that the toric graph can be decomposed into only two distinct subgraphs: star graphs, where one vertex is connected to all other vertices and which define Greenberger-Horne-Zeilinger (GHZ) states [37] (see for example Fig. 1a), and half graphs [38] (see for example Fig. 1b). Perhaps surprisingly, the macroscopic distance of the toric code is identified with the existence of multiple star subgraphs. Despite the fact that the number of edges in the toric code graph increases as L^2 , the binary quadratic function defining the graph adjacency matrix [39] is shown to be decomposable into a $\log(N)$ number of operations. Using this insight, we provide an explicit quantum algorithm to generate toric graph states in log depth. Furthermore, because any graph state can be generated in constant depth by including ancillae that are subsequently projected out via measurements [40], our algorithm can be expressed in constant depth at the cost of increasing the circuit width from scaling as N to scaling as $L^3 \sim N^{3/2}$. Given the result in Ref. [17], this work therefore provides an algorithm for the preparation of any 2D topological stabilizer code state in either log depth including only unitary gates or in constant depth allowing for measurements of ancillae.

This manuscript is organized as follows. The technical background is reviewed in Sec. II. The mapping of the

toric code stabilizer to the graph is covered in Sec. III, and the resulting graph structure and its decomposition are discussed. Section IV covers the construction of the log-depth quantum circuit that generates a toric graph state and its generalization for the preparation of any 2D topological stabilizer code state. The results are discussed briefly in Sec. V. Various technical details and proofs are included in the Appendices.

II. BACKGROUND AND FORMALISM

A. Stabilizer states and graph states

Define the Pauli group on N qubits as $\mathcal{P}_N := \{\pm 1, \pm i\} \times \{I, X, Y, Z\}^{\otimes N}$, where

$$X = \begin{pmatrix} 0 & 1 \\ 1 & 0 \end{pmatrix}; \quad Y = \begin{pmatrix} 0 & -i \\ i & 0 \end{pmatrix}; \quad Z = \begin{pmatrix} 1 & 0 \\ 0 & -1 \end{pmatrix} \quad (1)$$

correspond to the Pauli matrices. The set $\mathcal{S} := \{S \in \mathcal{P}_N \mid S|\psi\rangle = |\psi\rangle\}$ is said to stabilize a state $|\psi\rangle \in \mathcal{H}_2^{\otimes N}$. The set of states simultaneously stabilized by m independent operators $\{S_1, \dots, S_m\}$ from \mathcal{P}_N then generate a state subspace of dimension 2^{N-m} . When $m = N$, the subspace contains only one state called the stabilizer state, and the N independent operators are the generators of \mathcal{S} .

Graph states are special stabilizer states where the stabilizer generators are related to simple graphs [37]. Given a graph $G = (V, E)$, where $|V| = N$, the corresponding graph state is

$$|G\rangle = \prod_{\substack{(i,j) \in E \\ i < j}} \text{CZ}(i,j) H^{\otimes N} |0^N\rangle, \quad (2)$$

for which the stabilizer generators are

$$S_i = X_i \prod_{(i,j) \in E} Z_j. \quad (3)$$

Associating the graph to its adjacency matrix A , the graph state can also be written in terms of its binary quadratic form [39]

$$|G\rangle = \frac{1}{\sqrt{2^N}} \sum_{q \in \{0,1\}^N} (-1)^{f_G(q)} |q\rangle, \quad (4)$$

in which $f_G(q) = \sum_{i < j} A_{ij} q_i q_j \pmod{2}$ is a quadratic Boolean function. Unless stated otherwise, the addition on binary variables are all performed by $\pmod{2}$. There is therefore a useful correspondence among simple graphs, graph states, and quadratic Boolean functions.

As discussed in Sec. III, the toric code maps to a graph, called the toric graph in what follows, that can be decomposed into two types of subgraphs: star and half graphs. These are reviewed here, and examples are shown in Fig. 1. The star graph on m vertices is the

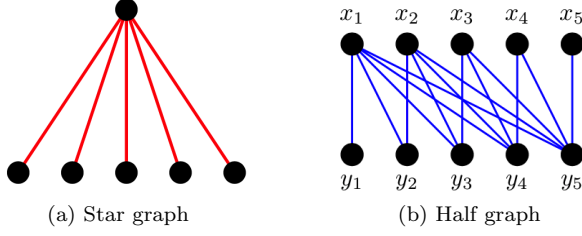


FIG. 1. (Color online) The two graphs comprising the toric graph.

complete bipartite graph $K_{m-1,1}$, as shown in Fig 1a. Because the star graph is LC-equivalent to the complete graph K_m [37], the label of the large-degree vertex is arbitrary. Without loss of generality, the non-zero elements of the adjacency matrix are then $A_{mi} = A_{im} = 1$ for $i = 1, \dots, m-1$, or alternatively

$$A_{ij}^{(\text{star})} = \delta_{i,m}\theta_{j,m-1} + \delta_{j,m}\theta_{i,m-1}, i, j \in \{1, \dots, m\}, \quad (5)$$

where $\delta_{i,j}$ and $\theta_{i,j}$ are the usual Kronecker and Heaviside theta functions, respectively:

$$\delta_{i,j} = \begin{cases} 1 & j = i \\ 0 & \text{otherwise} \end{cases} \quad \text{and} \quad \theta_{i,j} = \begin{cases} 1 & i \leq j \\ 0 & \text{otherwise} \end{cases}. \quad (6)$$

The star graph state can then be written as

$$\begin{aligned} |G_{\text{star}}\rangle &= \frac{|+\rangle^{\otimes m-1} |0\rangle + |-\rangle^{\otimes m-1} |1\rangle}{\sqrt{2}} \\ &= \frac{1}{\sqrt{2^m}} \sum_{q \in \{0,1\}^m} (-1)^{f_{\text{star}}(q)} |q\rangle, \end{aligned} \quad (7)$$

where $f_{\text{star}}(q) = (q_1 + \dots + q_{m-1}) \cdot q_m = q_m P(q_{m-1})$; here P is the parity operator acting on the length $m-1$ bit string $q_{m-1} \equiv q_1 \oplus \dots \oplus q_{m-1}$. Evidently, $|G_{\text{star}}\rangle$ is locally equivalent to an m -qubit GHZ state

$$I^{\otimes m-1} \otimes H |G_{\text{star}}\rangle = \frac{|+\rangle^{\otimes m} + |-\rangle^{\otimes m}}{\sqrt{2}}. \quad (8)$$

The second example is the half graph $K_{n,n}^{(\text{half})}$ (our notation), a $2n$ -vertex balanced bipartite graph where the n vertices x_i ($i = 1, \dots, n$) in one bipartition share an edge with the n vertices y_j ($j = 1, \dots, n$) in the other whenever $i \leq j$. An example is shown in Fig. 1b. Alternatively, the non-zero entry of the adjacency matrix can be written as

$$A_{x_i y_j}^{(\text{half})} = \theta_{i,j}, \quad i \in \{1, \dots, n\}, j \in \{1, \dots, n\}. \quad (9)$$

The corresponding graph state can be written as

$$|K_{n,n}^{(\text{half})}\rangle = \frac{1}{\sqrt{2^{2n}}} \sum_{q,p \in \{0,1\}^n} (-1)^{f_{\text{half}}(q,p)} |q,p\rangle, \quad (10)$$

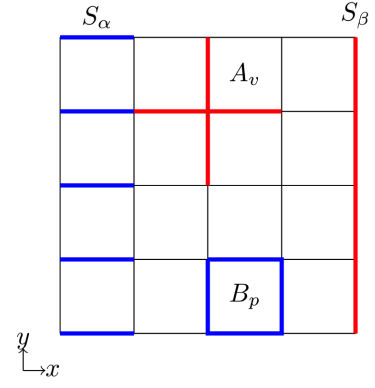


FIG. 2. (Color online) Representation of operators in the 2D toric code. Qubits reside on the edges of the lattice (not shown), on which X and Z gates are applied (red and blue lines, respectively). The red plus and blue square represent the star A_v and plaquette B_p operator, respectively; the corresponding string operators S_β and S_α are also depicted.

where the associated quadratic function is $f_{\text{half}}(q,p) = \sum_{i \leq j} q_i p_j$.

One can directly use Eq. (2) to construct the quantum circuit to generate an arbitrary graph state $|G\rangle$. As the CZ gates share no common qubits, they can all be implemented in parallel, yielding a $\Delta(G)$ -depth circuit [40], where $\Delta(G)$ is the (maximum) vertex degree of the graph. For the n -vertex star graph and $2n$ -vertex half graph discussion above, preparing the corresponding graph states then seems to require a $O(n)$ -depth quantum circuit. In fact, as we show below, these two special graph states can be generated with a log-depth quantum circuit.

B. 2D toric code

The toric code on a square lattice is defined on an $L \times L$ grid with periodic boundary conditions in both directions, so that the system geometry corresponds to a two-torus. A physical qubit is placed on every edge, so that there are a total of $N = 2L^2$ qubits. The stabilizer generators are

$$A_v = \prod_{i \in v} \sigma_i^x, \quad B_p = \prod_{i \in p} \sigma_i^z, \quad (11)$$

where the first sum is over the nearest qubits surrounding a given vertex v of the lattice, corresponding to a ‘star’ operator, while the second is over the nearest qubits surrounding the center p of a square, corresponding to a ‘plaquette’ operator. These operators are depicted in Fig 2.

The star and plaquette operators can share at most two edges, so that the A_v and B_p commute. However, they are not entirely independent because

$$\prod_v A_v = I, \quad \prod_p B_p = I, \quad (12)$$

where I is the identity. There are $N - 2$ independent stabilizer generators and the ground subspace of the associated Hamiltonian

$$H = - \sum_v A_v - \sum_p B_p \quad (13)$$

is four-fold degenerate. In order to specify one state in the degenerate subspace, we add two more stabilizer generators S_α and S_β . One choice for the S_α (S_β) corresponds to a string of Z (X) gates applied to the qubits residing only on vertical (horizontal) edges of a given column of the lattice. The choice of column is unimportant because of the translational invariance of the system; also, the columns for S_α and S_β can coincide because the operations are on a different set of qubits. For the same reason, the S_α and S_β strings can be oriented along either columns or rows. Each of the four different possible combinations yields one of the toric-code stabilizer states.

C. Local Clifford equivalence and the symplectic representation

In this work, we make heavy use of the symplectic representation of Pauli operators [16]. As this formalism is not widely employed, we briefly review the notation here, closely following the notation in Ref. [36]. Neglecting overall phases, a single Pauli matrix (1) can be written as $\sigma = Z^u X^v$, where $u, v \in \{0, 1\}$. Alternatively, they can be represented as a binary tuple, $I \rightarrow (0|0)$, $X \rightarrow (0|1)$, $Z \rightarrow (1|0)$, and $Y \rightarrow (1|1)$ or equivalently the vectors

$$I = \begin{pmatrix} 0 \\ 0 \end{pmatrix}; \quad X = \begin{pmatrix} 0 \\ 1 \end{pmatrix}; \quad Y = \begin{pmatrix} 1 \\ 1 \end{pmatrix}; \quad Z = \begin{pmatrix} 1 \\ 0 \end{pmatrix}. \quad (14)$$

The generalization to N qubits $\sigma_1 \otimes \cdots \otimes \sigma_N$ is then $(u_1 \dots u_N | v_1 \dots v_N) \in \mathbb{Z}_2^{2N}$, i.e., a $2N$ -dimensional binary vector. For example,

$$X \otimes Z = (01|10) = \begin{pmatrix} 0 \\ 1 \\ 1 \\ 0 \end{pmatrix}. \quad (15)$$

The N stabilizer generators that uniquely define an N -qubit state can then be expressed as full-rank $2N \times N$ -dimensional matrix S ; for example, the graph state corresponding to the two-vertex path graph P_2 is defined by the stabilizer generators $S_1 = X \otimes Z$ and $S_2 = Z \otimes X$, which are combined in the symplectic notation:

$$S_{P_2} = \begin{pmatrix} 0 & 1 \\ 1 & 0 \\ 1 & 0 \\ 0 & 1 \end{pmatrix} = \begin{pmatrix} A \\ I \end{pmatrix}, \quad (16)$$

where A is the associated graph adjacency matrix. This standard form for the stabilizer code is equivalent to the

parity-check matrix in error correction. The central advantage of this formulation is that, because all of the stabilizer generators are mutually commuting, the matrix S is automatically self-orthogonal under the symplectic inner product $S^T J S = 0$, where

$$J = \begin{pmatrix} \mathbf{0} & I \\ I & \mathbf{0} \end{pmatrix} \quad (17)$$

is the symplectic metric tensor (note that the sign convention is not the same as the symplectic algebra in classical Hamiltonian mechanics), and $\mathbf{0}$ represents the all-zero matrix.

Clifford operations, which maps the Pauli group to itself under conjugation, then correspond to $2N \times 2N$ matrices Q that preserve the metric, i.e. $Q^T J Q = J$ [41]. Local Clifford gates refer to those which are tensor products of local gates acting on single qubits. Two quantum states are local Clifford equivalent if they can be mapped to each other by local Clifford operations. Clifford operations that transform a stabilizer generator matrix S to another S' can always be written in the form $S' = QSR$, where R is an $N \times N$ invertible matrix corresponding to a basis change [36]. Restricting to local Clifford gates further implies that Q can be partitioned into four $N \times N$ blocks, each of which is diagonal. For example, if we partition all qubits into two complementary sets $R_1 \cup R_2 = \{1, \dots, N\}$, then

$$H_{R_2} = \bigotimes_{i \in R_1} I \bigotimes_{j \in R_2} H_j \quad (18)$$

is a local Clifford operation and its symplectic representation is

$$Q = \begin{pmatrix} I_{R_1} & \mathbf{0} & \mathbf{0} & \mathbf{0} \\ \mathbf{0} & \mathbf{0} & \mathbf{0} & I_{R_2} \\ \mathbf{0} & \mathbf{0} & I_{R_1} & \mathbf{0} \\ \mathbf{0} & I_{R_2} & \mathbf{0} & \mathbf{0} \end{pmatrix}. \quad (19)$$

The transformation of the stabilizer is then effected by ordinary matrix-vector multiplication. These results imply a specific procedure to map any stabilizer generator matrix to standard (graph) form, which is used in this work to derive the (non-unique) graph that stabilizes the toric code.

III. TORIC GRAPH STATE

In this section, we first introduce the symplectic representation of toric code. Then we show how to obtain toric graph state from the ground state in toric code specified by two string operators. Next, we present the decomposition of toric graph and prove that subgraph consisting of multiple star graphs contribute to the macroscopic distance of the toric code.

A. Symplectic representation of the toric code

In the toric code, qubits are located on the edges of a regular $L \times L$ square lattice thus there are $N = 2L^2$ qubits in total. It is convenient to distinguish the qubits situated on horizontal (x) and vertical (y) edges, whose locations on the grid are denoted by (i, j, x) and (i, j, y) , respectively, where $i, j \in \{1, L\}$. The star operator A_v^{ij} centered at coordinate (i, j) then includes qubits with labels $\{(i-1, j, x), (i, j, x), (i, j-1, y), (i, j, y)\} \bmod L$; likewise, the plaquette operator B_p^{ij} with the coordinate (i, j) located at the top left of a given plaquette includes qubits with labels $\{(i, j, x), (i, j+1, x), (i, j, y), (i+1, j, y)\} \bmod L$. Given that the star and plaquette terms apply X and Z gates, respectively, they can be expressed in the symplectic representation as

$$A_{\text{bin}}^{ij} = \begin{pmatrix} 0 \\ v^{ij} \end{pmatrix}; \quad B_{\text{bin}}^{ij} = \begin{pmatrix} p^{ij} \\ 0 \end{pmatrix}, \quad (20)$$

where $A_{\text{bin}}^{ij}, B_{\text{bin}}^{ij}$ are $4L^2$ -length vectors, and $v^{ij}, p^{ij} \in \mathbb{Z}_2^{2L^2}$ are binary strings with elements defined by

$$\begin{aligned} v_{lmd}^{ij} &= \delta_{i,l} \delta_{j,m} + \delta_{i-1,l} \delta_{j,m} \delta_{d,x} + \delta_{i,l} \delta_{j-1,m} \delta_{d,y}; \\ p_{lmd}^{ij} &= \delta_{i,l} \delta_{j,m} + \delta_{i,l} \delta_{j+1,m} \delta_{d,x} + \delta_{i+1,l} \delta_{j,m} \delta_{d,y}, \end{aligned} \quad (21)$$

where $l, m \in \{1, \dots, L\}$ and $d \in \{x, y\}$. The toric code stabilizer, without the string operators, therefore consists of the antidiagonal block matrix

$$S = \begin{pmatrix} \mathbf{0} & Z_p \\ X_v & \mathbf{0} \end{pmatrix}, \quad (22)$$

where the columns of the $2L^2 \times L^2$ matrices X_v and Z_p correspond respectively to the v^{ij} and p^{ij} , $i, j \in \{1, L\}$.

With the expressions (21), it is straightforward to prove the relations (12) within the symplectic notation:

$$\prod_v A_v = \prod_v \begin{pmatrix} \mathbf{0} \\ X_v \end{pmatrix} = \begin{pmatrix} \mathbf{0} \\ \sum_{ij} v^{ij} \end{pmatrix}. \quad (23)$$

Note that evaluation of the terms in the sum above (and in what follows) is accomplished via bitwise exclusive or (XOR), with $0+0=1+1=0$ and $0+1=1+0=1$. The resulting bitstring is then

$$\begin{aligned} \sum_{ij} v^{ij} &= \sum_{ij} \bigoplus_{lmd} v_{lmd}^{ij} \\ &= \bigoplus_{lmd} \sum_{ij} (\delta_{i,l} \delta_{j,m} + \delta_{i-1,l} \delta_{j,m} \delta_{d,x} + \delta_{i,l} \delta_{j-1,m} \delta_{d,y}) \\ &= \bigoplus_{lm} \left(\bigoplus_d 1 + \bigoplus_d \delta_{d,x} + \bigoplus_d \delta_{d,y} \right) = \mathbf{0}, \end{aligned} \quad (24)$$

which yields

$$\prod_v A_v = \begin{pmatrix} \mathbf{0} \\ \mathbf{0} \end{pmatrix} = I, \quad (25)$$

as expected. The second condition in Eq. (12) is found analogously. Note that in this work, the \oplus notation represents a direct sum rather than an XOR operation.

B. Star operators

To bring the stabilizer (22) into the standard form, the $2L^2 \times 2L^2$ submatrix $(0|X_v)$ must be transformed into an identity. Due to the constraint (12), the rank of X_v is only $L^2 - 1$. The first step in the procedure is to form a full-rank $L^2 - 1$ -dimensional matrix by taking linear combinations of the X_v vectors to obtain a zero column vector. This column is replaced by S_β , and finally column permutations yield an $L^2 \times L^2$ identity submatrix. The remaining $L^2 \times L^2$ identity submatrix will be obtained from the plaquette operators, Sec. III C.

The first linear combination is achieved by multiplying X_v on the right by $R^x T^x$, where $T^x, R^x \in \mathbb{Z}_2^{L^2 \times L^2}$ are invertible matrices with elements defined by

$$\begin{aligned} R_{kn,ij}^x &= \theta_{i,k} \delta_{j,n}; \\ T_{kn,ij}^x &= \begin{cases} \delta_{i,k} \theta_{j,n} & i = 1 \\ \delta_{i,k} \delta_{j,n} & \text{otherwise.} \end{cases} \end{aligned} \quad (26)$$

Consider first the action of R^x . The column vectors of $X_v R^x$ are

$$\begin{aligned} v^{ij'} &= \sum_{kn} v^{kn} R_{kn,ij}^x = \sum_{kn} v^{kn} \theta_{i,k} \delta_{j,n} = \sum_{k=i}^L v^{kj} \\ &= \bigoplus_{lmd} \sum_{k=i}^L (\delta_{k,l} \delta_{j,m} + \delta_{k-1,l} \delta_{j,m} \delta_{d,x} + \delta_{k,l} \delta_{j-1,m} \delta_{d,y}) \\ &= \bigoplus_{lmx} \sum_{k=i}^L \delta_{j,m} (\delta_{k,l} + \delta_{k-1,l}) \\ &\quad + \bigoplus_{lmy} \sum_{k=i}^L \delta_{k,l} (\delta_{j,m} + \delta_{j-1,m}). \end{aligned} \quad (27)$$

Let's evaluate the first term above:

$$\begin{aligned} &\bigoplus_{lmx} \sum_{k=i}^L \delta_{j,m} (\delta_{k,l} + \delta_{k-1,l}) \\ &= \bigoplus_{lmx} \delta_{j,m} (\delta_{i,l} + \delta_{i-1,l} + \delta_{i+1,l} + \delta_{i,l} \\ &\quad + \dots + \delta_{L-1,l} + \delta_{L-2,l} + \delta_{L,l} + \delta_{L-1,l}) \\ &= \bigoplus_{lmx} \delta_{j,m} (\delta_{i-1,l} + \delta_{L,l}), \end{aligned} \quad (28)$$

where only the endpoints in the sum are unpaired and therefore remain. One then obtains the matrix elements

$$\begin{aligned} v_{lmd}^{ij'} &= (\delta_{L,l} + \delta_{i-1,l}) \delta_{d,x} \delta_{j,m} \\ &\quad + \theta_{i,l} (\delta_{j,m} + \delta_{j-1,m}) \delta_{d,y}. \end{aligned} \quad (29)$$

Next consider the action of T^x :

$$\begin{aligned} v^{ij''} &= \sum_{kn} v^{kn'} T_{kn,ij}^x \\ &= \sum_{kn} v^{kn'} \delta_{i,k} \times \begin{cases} \theta_{j,n} & i = 1 \\ \delta_{j,n} & \text{otherwise} \end{cases} \end{aligned} \quad (30)$$

which equals $v^{ij'}$ when $i \neq 1$, but for $i = 1$ one obtains

$$v^{1j''} = \sum_{n=j}^L v^{1n'}. \quad (31)$$

Using Eq. (29) and the fact that $i-1 = L$ when $i = 1$ due to the periodic boundary conditions, the matrix elements become

$$\begin{aligned} v_{lmd}^{1j''} &= \sum_{n=j}^L \delta_{d,y} (\delta_{n,m} + \delta_{n-1,m}) \theta_{1,l} \\ &= \delta_{d,y} (\delta_{L,m} + \delta_{j-1,m}). \end{aligned} \quad (32)$$

Again because of the periodic boundary conditions, $v^{11''} = \mathbf{0}$, which shows explicitly that the rank of $X_v R^x T^x$ is reduced by one. In order to make X_v a full-rank matrix, the zero column is replaced by the string operator $S_\beta = (\mathbf{0}|s_\beta)$, where $s_\beta = \bigoplus_{lmd} \delta_{d,y} \delta_{L,m}$. One then obtains

$$v^{1j'''} = v^{1j+1''} + s_\beta = \bigoplus_{lmd} \delta_{d,y} \delta_{j,m}. \quad (33)$$

All other column vectors remain unchanged: $v^{ij'''} = v^{ij''}$ when $i \neq 1$.

It remains to show that one can extract an $L^2 \times L^2$ identity submatrix from X_v''' , whose columns are the $v^{ij'''}$. Consider two complementary subsets of row indices R_1 and R_2 , defined as

$$\begin{aligned} R_1 &:= \{1, \dots, L-1\}_x \times \{1, \dots, L\}_y \\ &\cup \{1\}_y \times \{1, \dots, L\}_y; \\ R_2 &:= \{L\}_x \times \{1, \dots, L\}_x \\ &\cup \{2, \dots, L\}_y \times \{1, \dots, L\}_y, \end{aligned} \quad (34)$$

where $\{\dots\}_d \times \{\dots\}_d$ represents the row and column indices of the original square lattice and d indicates a horizontal x or vertical y qubit. Clearly, both R_1 and R_2 contain L^2 rows. Combining the results of Eqs. (29) and (33), one obtains the elements

$$\begin{aligned} v_{lmdR_1}^{ij'''} &= \delta_{j,m} \times \begin{cases} \delta_{i,l} \delta_{d,y} & i = 1 \\ \delta_{i-1,l} \delta_{d,x} & i \geq 2; \end{cases} \\ v_{lmdR_2}^{ij'''} &= \begin{cases} \theta_{2,l} \delta_{j,m} \delta_{d,y} & i = 1 \\ \delta_{L,l} \delta_{j,m} \delta_{d,x} + \theta_{i,l} (\delta_{j,m} + \delta_{j-1,m}) \delta_{d,y} & i \geq 2. \end{cases} \end{aligned} \quad (35)$$

There is only one non-zero element in each bitstring $v_{R_1}^{ij'''}$ and its location is unique. Therefore, X_v''' is an $L^2 \times L^2$ identity matrix after appropriate permutation of columns, which will be effected in Sec. IIID.

C. Plaquette operators

The plaquette operators are treated in much the same way as the star operators discussed in Sec. IIIB: form

linear combinations of the Z_p column vectors to obtain a zero column vector, then replace this with the string operator S_α to make Z_p a full-rank matrix, and finally use linear combinations again to extract an $L^2 \times L^2$ submatrix.

Define invertible operators $T^z, R^z \in \mathbb{Z}_2^{L^2 \times L^2}$ with elements

$$R_{kn,ij}^z = \theta_{k,i} \delta_{j,n}; \quad (36)$$

$$T_{kn,ij}^z = \delta_{i,k} \begin{cases} \theta_{n,j} & i = L \\ \delta_{n,j} & \text{otherwise.} \end{cases} \quad (37)$$

The column vector of $Z_p R^z$ is

$$\begin{aligned} p^{ij'} &= \sum_{kn} p^{kn} R_{kn,ij}^z = \sum_k p^{kj} \theta_{k,i} = \sum_{k=1}^i p^{kj} \\ &= \bigoplus_{lmd} \sum_{k=1}^i (\delta_{k,l} \delta_{j,m} + \delta_{k,l} \delta_{j+1,m} \delta_{d,x} + \delta_{k+1,l} \delta_{j,m} \delta_{d,y}) \\ &= \bigoplus_{lmx} (\delta_{j,m} + \delta_{j+1,m}) \sum_{k=1}^i \delta_{k,l} \\ &\quad + \bigoplus_{lmy} \delta_{j,m} \sum_{k=1}^i (\delta_{k,l} + \delta_{k+1,l}) \\ &= \bigoplus_{lmd} \theta_{l,i} (\delta_{j,m} + \delta_{j+1,m}) \delta_{d,x} + (\delta_{1,l} + \delta_{i+1,l}) \delta_{j,m} \delta_{d,y}. \end{aligned} \quad (38)$$

The column vector of $Z_p R^z T^z$ is $p^{ij''} = p^{ij'}$ when $i \neq L$. When $i = L$, one can make use of the periodic boundary conditions to obtain

$$\begin{aligned} p^{Lj''} &= \sum_{kn} p^{kn'} T_{kn,Lj}^z = \sum_n p^{Ln'} \theta_{n,j} = \sum_{n=1}^j p^{Ln'} \\ &= \bigoplus_{lmd} \sum_{n=1}^j (\delta_{n,m} + \delta_{n+1,m}) \theta_{l,L} \delta_{d,x} \\ &= \bigoplus_{lmd} (\delta_{1,m} + \delta_{j+1,m}) \delta_{d,x}. \end{aligned} \quad (39)$$

Again, one obtains a zero vector, $p^{LL''} = \mathbf{0}$. In order to yield a full-rank matrix for Z_p , we include the string operator $S_\alpha = (s_\alpha|\mathbf{0})$, where $s_\alpha = \bigoplus_{lmd} \delta_{d,x} \delta_{m,1}$. Then

$$p^{Lj'''} = p^{L,j-1''} + s_\alpha = \bigoplus_{lmd} \delta_{j,m} \delta_{d,x}. \quad (40)$$

All other column vectors remain unchanged: $p^{ij'''} = p^{Lj''}$ when $i \neq L$.

The column vector of matrix Z_p''' is $p^{ij'''}$, from which one can extract another $L^2 \times L^2$ identity submatrix. Again using the complementary subsets of row indices R_1 and R_2 , Eq. (34), the elements of the plaquette bit-

strings become

$$p_{lmdR_1}^{ij} = \begin{cases} \theta_{l,i}(\delta_{j,m} + \delta_{j+1,m})\delta_{d,x} + \delta_{1,l}\delta_{j,m}\delta_{d,y} & i < L \\ \theta_{l,L-1}\delta_{j,m}\delta_{d,x} & i = L; \end{cases}$$

$$p_{lmdR_2}^{ij} = \delta_{j,m} \times \begin{cases} \delta_{i+1,l}\delta_{d,y} & i < L \\ \delta_{l,L}\delta_{d,x} & i = L. \end{cases} \quad (41)$$

As was the case for the star operators, there is only one non-zero element in each bitstring $v_{R_2}^{ij}$ and its location is unique. Therefore, $Z_{p_{R_2}}'''$ is another $L^2 \times L^2$ identity matrix after appropriate permutation of columns, which will be effected in Sec. III D. Combining these results with those in Sec. III B), the toric code stabilizer in symplectic form, Eq. (22), is now transformed to

$$S \rightarrow \begin{pmatrix} \mathbf{0} & Z_{p_{R_2}}''' \\ X_v''' & \mathbf{0} \end{pmatrix} = \begin{pmatrix} \mathbf{0} & Z_{p_{R_1}}''' \\ X_{v_{R_1}}''' & \mathbf{0} \\ X_{v_{R_2}}''' & \mathbf{0} \end{pmatrix}. \quad (42)$$

D. Transformation to standard form

To convert the stabilizer (42) to standard form, one first applies Hadamard operations to the R_2 qubits,

$$Q \begin{pmatrix} \mathbf{0} & Z_{p_{R_2}}''' \\ X_v''' & \mathbf{0} \end{pmatrix} = \begin{pmatrix} \mathbf{0} & Z_{p_{R_1}}''' \\ X_{v_{R_2}}''' & \mathbf{0} \\ X_{v_{R_1}}''' & Z_{p_{R_2}}''' \end{pmatrix} = \begin{pmatrix} A \\ B \end{pmatrix}, \quad (43)$$

where Q is defined in Eq. (19). It remains to convert B to a $2L^2 \times 2L^2$ identity matrix, which is accomplished by appropriate column permutations. The columns of B , expressed as b^{ij} , are $v_{R_1}^{ij} \oplus \mathbf{0}_{R_2}$ and $\mathbf{0}_{R_1} \oplus p_{lmdR_2}^{ij}$, where according to Eqs. (35) and (41)

$$v_{lmdR_1}^{ij} = \delta_{j,m} \times \begin{cases} \delta_{i,l}\delta_{d,y} & i = 1 \\ \delta_{i-1,l}\delta_{d,x} & i \geq 2; \end{cases}$$

$$p_{lmdR_2}^{ij} = \delta_{j,m} \times \begin{cases} \delta_{i+1,l}\delta_{d,y} & i < L \\ \delta_{l,L}\delta_{d,x} & i = L, \end{cases} \quad (44)$$

and these are to be converted to the matrix elements of the identity

$$b_{lmd_2}^{ijd_1} = \delta_{i,l}\delta_{j,m}\delta_{d_1,d_2}, \quad (45)$$

where $i, j, l, m \in \{1, \dots, L\}$ and $d_1, d_2 \in \{x, y\}$.

When $i \in \{2, \dots, L\}$, the column vector of B is

$$v_{R_1}^{ij} \oplus \mathbf{0}_{R_2} = \bigoplus_{lmd \in R_1} \delta_{i-1,l}\delta_{j,m}\delta_{d,x} \oplus \bigoplus_{lmd \in R_2} 0$$

$$= \bigoplus_{lmx} \delta_{i-1,l}\delta_{j,m}, \quad (46)$$

where the only nonzero entry is at row $(i-1, j, x)$. To map to the form in Eq. (45), relabel this column vector:

$$b^{ijx} = v_{R_1}^{i+1,j} \oplus \mathbf{0}_{R_2} = \bigoplus_{lmd} \delta_{i,l}\delta_{j,m}\delta_{d,x}, \quad (47)$$

where now $i \in \{1, \dots, L-1\}$. Any column permutation on B must also be performed on A . Recall from Eqs. (35) and (41) that the columns of A , expressed as a^{ij} , are expressed as $p_{R_1}^{ij} \oplus \mathbf{0}_{R_2}$ and $\mathbf{0}_{R_1} \oplus v_{R_2}^{ij}$, with elements

$$p_{lmdR_1}^{ij} = \begin{cases} \theta_{l,i}(\delta_{j,m} + \delta_{j+1,m})\delta_{d,x} + \delta_{1,l}\delta_{j,m}\delta_{d,y} & i < L \\ \theta_{l,L-1}\delta_{j,m}\delta_{d,x} & i = L; \end{cases}$$

$$v_{lmdR_2}^{ij} = \begin{cases} \theta_{2,l}\delta_{j,m}\delta_{d,y} & i = 1 \\ \delta_{L,l}\delta_{j,m}\delta_{d,x} + \theta_{i,l}(\delta_{j,m} + \delta_{j-1,m})\delta_{d,y} & i \geq 2. \end{cases} \quad (48)$$

From Eq. (43), the column vector in A with the same column index as $v_{R_1}^{ij} \oplus \mathbf{0}_{R_2}$ is $\mathbf{0}_{R_1} \oplus v_{R_2}^{ij}$. Then

$$a^{ijx} = \mathbf{0}_{R_1} \oplus v_{R_2}^{i+1,j}$$

$$= \bigoplus_{lmd} \delta_{L,l}\delta_{j,m}\delta_{d,x} + \theta_{i+1,l}(\delta_{j,m} + \delta_{j-1,m})\delta_{d,y}, \quad (49)$$

again with $i \in \{1, \dots, L-1\}$. Likewise, when $i = L$:

$$b^{Ljx} = \mathbf{0}_{R_1} \oplus p_{R_2}^{Lj} = \bigoplus_{lmd} \delta_{l,L}\delta_{j,m}\delta_{d,x}, \quad (50)$$

$$a^{Ljx} = p_{R_1}^{Lj} \oplus \mathbf{0}_{R_2} = \bigoplus_{lmd} \theta_{l,L-1}\delta_{j,m}\delta_{d,x}; \quad (51)$$

when $i \in \{2, \dots, L\}$:

$$b^{ijy} = \mathbf{0}_{R_1} \oplus p_{R_2}^{i-1,j} = \bigoplus_{lmd} \delta_{i,l}\delta_{j,m}\delta_{d,y}, \quad (52)$$

$$a^{ijy} = p_{R_1}^{i-1,j} \oplus \mathbf{0}_{R_2}$$

$$= \bigoplus_{lmd} \theta_{l,i-1}(\delta_{j,m} + \delta_{j+1,m})\delta_{d,x} + \delta_{1,l}\delta_{j,m}\delta_{d,y}; \quad (53)$$

and when $i = 1$:

$$b^{1jy} = v_{R_1}^{1j} \oplus \mathbf{0}_{R_2} = \bigoplus_{lmd} \delta_{1,l}\delta_{j,m}\delta_{d,y}, \quad (54)$$

$$a^{1jy} = \mathbf{0}_{R_1} \oplus v_{R_2}^{1j} = \bigoplus_{lmd} \theta_{2,l}\delta_{j,m}\delta_{d,y}. \quad (55)$$

That B is an identity matrix after column permutations is clear from Eqs. (47), (50), (52), and (54).

Finally, the adjacency matrix A for the toric code graph is obtained by combining Eqs. (49), (51), (53), and (55):

$$a_{lmd_2}^{ijd_1} = \delta_{d_1,x}\delta_{d_2,x}\delta_{m,j}(\delta_{l,L}\theta_{i,L-1} + \delta_{i,L}\theta_{l,L-1})$$

$$+ \delta_{d_1,y}\delta_{d_2,y}\delta_{m,j}(\delta_{i,1}\theta_{2,l} + \delta_{l,1}\theta_{2,i})$$

$$+ \delta_{d_1,y}\delta_{d_2,x}(\delta_{m,j} + \delta_{m-1,j})\theta_{l,i-1}\theta_{2,i}$$

$$+ \delta_{d_1,x}\delta_{d_2,y}(\delta_{m,j} + \delta_{j-1,m})\theta_{i+1,l}\theta_{i,L-1}. \quad (56)$$

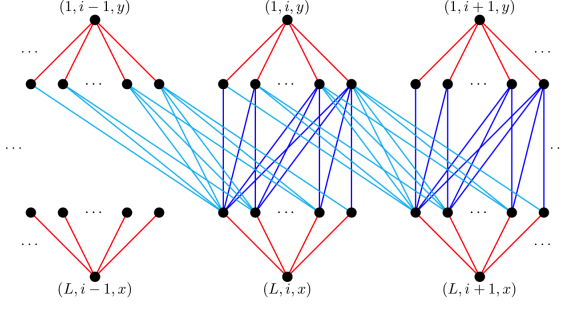


FIG. 3. (Color online) A portion of the toric graph. Shown are the multiple star graphs with central vertices labeled by $(1, j, y)$ and (L, j, x) qubits, each connected to the remaining $L-1$ vertices labeled by (i, j, y) ($i \in [2, L]$) and (i', j, x) ($i' \in [1, L-1]$), respectively. Also shown are two of the half1 graphs that connect the (i, j, y) and (i', j, x) vertices, and two of the half2 graphs that connect the (i, j, y) and (i', j, x) vertices.

Note that the matrix elements in the expression above are symmetric under $i \leftrightarrow l$ and $j \leftrightarrow m$; the apparent lack of symmetry in the last two lines is resolved by noting that

$$\theta_{i+1,l}\theta_{i,L-1} = \theta_{i,l-1}\theta_{2,l}\theta_{i,L-1} = \theta_{i,l-1}\theta_{2,l}. \quad (57)$$

Eq. (56) is the first of two key results of the present work. The graph represented by the adjacency matrix will be referred to as the toric graph, illustrated in Fig 3, and the corresponding graph state is called the toric graph state.

The result (56) was checked in two ways. First, the graph state for small systems was generated explicitly and compared with the toric code state on the same number of qubits. Second, the reduced density matrices and entanglement entropies for various bipartitions of the two systems were compared and found to agree in all cases.

E. Decomposition of the toric graph

The elements of the graph adjacency matrix, Eq. (56), and the associated graph shown in Fig 3, appear too complicated to gain any insights about why this particular structure corresponds to a topological quantum state. However, it turns out this graph can be decomposed into three subgraphs, all of which have a rather simple structure. In particular, the adjacency matrix given can be decomposed into three terms:

$$A = A^{\text{mstar}} + A^{\text{mhalf1}} + A^{\text{mhalf2}}, \quad (58)$$

where the entries of those three matrices are

$$\begin{aligned} A_{i_1 j_1 d_1, i_2 j_2 d_2}^{\text{mstar}} &= \delta_{d_1, y} \delta_{d_2, y} \delta_{j_1, j_2} (\delta_{i_2, 1} \theta_{2, i_1} + \delta_{i_1, 1} \theta_{2, i_2}) \\ &\quad + \delta_{d_1, x} \delta_{d_2, x} \delta_{j_1, j_2} (\delta_{i_1, L} \theta_{i_2, L-1} + \delta_{i_2, L} \theta_{i_1, L-1}); \\ A_{i_1 j_1 d_1, i_2 j_2 d_2}^{\text{mhalf1}} &= \delta_{d_1, x} \delta_{d_2, y} \delta_{j_1, j_2} \theta_{i_1, i_2-1} \theta_{2, i_2} \\ &\quad + \delta_{d_1, y} \delta_{d_2, x} \delta_{j_1, j_2} \theta_{i_2, i_1-1} \theta_{2, i_1}; \\ A_{i_1 j_1 d_1, i_2 j_2 d_2}^{\text{mhalf2}} &= \delta_{d_1, x} \delta_{d_2, y} \delta_{j_1-1, j_2} \theta_{i_1, i_2-1} \theta_{2, i_2} \\ &\quad + \delta_{d_1, y} \delta_{d_2, x} \delta_{j_2-1, j_1} \theta_{i_2, i_1-1} \theta_{2, i_1}. \end{aligned} \quad (59)$$

These three matrices corresponding to three subgraphs G_{mstar} , G_{mhalf1} , and G_{mhalf2} , respectively.

First consider the subgraph G_{mstar} and the subset of vertices

$$Q_{jd}^1 := \{1, \dots, L\}_d \times \{j\}_d, \quad (60)$$

following the notation of Eq. (34). Because of the restriction δ_{j_1, j_2} in the definition of A^{mstar} above, there is no edge in G_{mstar} connecting qubits in different subsets Q_{jd}^1 . There are $2L$ disconnected components in total, and the adjacency matrices of components Q_{jx}^1 and Q_{jy}^1 have elements

$$\begin{aligned} (A_{jx}^{\text{star}})_{i_1, i_2} &= A_{i_1 j x, i_2 j x}^{\text{star}} = \delta_{i_1, L} \theta_{i_2, L-1} + \delta_{i_2, L} \theta_{i_1, L-1}; \\ (A_{jy}^{\text{star}})_{i_1, i_2} &= A_{i_1 j y, i_2 j y}^{\text{star}} = \delta_{i_2, 1} \theta_{2, i_1} + \delta_{i_1, 1} \theta_{2, i_2} \end{aligned} \quad (61)$$

respectively. From Eq. (5), the induced subgraphs on Q_{jx}^1 and Q_{jy}^1 are L -vertex star graphs with (L, j, x) and $(1, j, y)$ being the central vertices, respectively, as shown in Fig 4a. Thus, ‘mstar’ is an abbreviation for ‘multiple star graphs.’

The graph G_{mhalf1} is similarly made up of L disconnected components, indexed by j . The adjacency matrix elements are

$$\begin{aligned} (A_j^{\text{mhalf1}})_{i_1 d_1, i_2 d_2} &= A_{i_1 j d_1, i_2 j d_2}^{\text{mhalf1}} \\ &= \delta_{d_1, x} \delta_{d_2, y} \theta_{i_1, i_2-1} \theta_{2, i_2} \\ &\quad + \delta_{d_1, y} \delta_{d_2, x} \theta_{i_2, i_1-1} \theta_{2, i_1}. \end{aligned} \quad (62)$$

When $i_1 = 1$, θ_{2, i_1} is always zero, so vertex $(1, j, y)$ is isolated; likewise $\theta_{i_1, i_2-1} \theta_{2, i_2}$ is always zero when $i_1 = L$ and (L, j, x) is also isolated. Based on Eqs. (62) and (9), G_{mhalf1} corresponds to multiple copies of a $2(L-1)$ -vertex half graph, as shown in Fig. 4b.

G_{mhalf2} is almost the same as G_{mhalf1} : composed of L disconnected components and each component is a $2(L-1)$ -vertex half graph. The only difference is that the vertices in each of the components are different:

$$Q_j^2 := \{1, \dots, L\}_d \times \left(\{j\}_y \cup \{j+1\}_x \right). \quad (63)$$

The adjacency matrix of induced subgraph on each component Q_j^2 is the same as in Eq. (62), and the graph is shown in Fig 4c.

F. Observations on the toric graph structure

As both the star and half graphs are bipartite, the toric graph is also bipartite. Though this representation is not

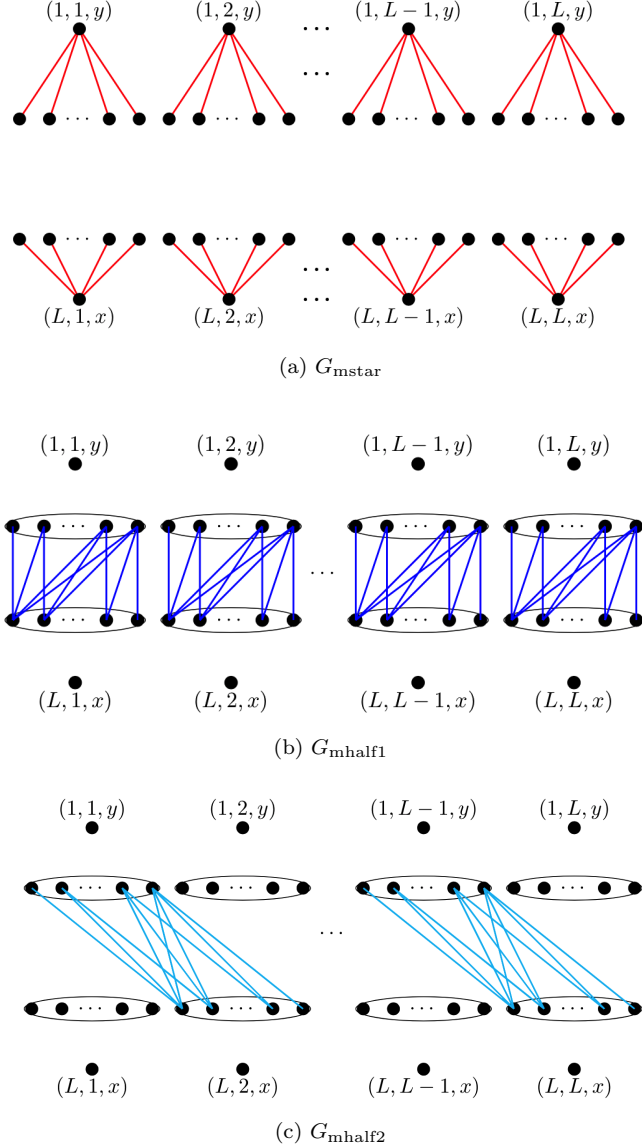


FIG. 4. (Color online) The three subgraphs of the toric graph.

unique (for example the choice of central vertex for the star graphs is arbitrary), the bipartiteness ensures that it has the fewest number of edges: any local Clifford map to another graph state is equivalent to a local edge complementation [36] that will generate an additional edge between two vertices within the same independent set. This representation is therefore the most efficient in terms of the size of the edge set.

As discussed in Sec. II A, the stabilizer state represented by the star graph is LC-equivalent to the GHZ state, so the graph state represented by G_{mstar} is LC-equivalent to multiple copies of the GHZ state. In fact, such a multiple-copy GHZ state is already ‘topologically ordered,’ in the sense that it is a code state in a quantum error correction code with macroscopic distance $d \sim \sqrt{N}$.

Consider two m -qubit GHZ states

$$|\phi_m^+\rangle = \frac{|0^m\rangle + |1^m\rangle}{\sqrt{2}}, \quad |\phi_m^-\rangle = \frac{|0^m\rangle - |1^m\rangle}{\sqrt{2}}. \quad (64)$$

and their m -copy states on m^2 qubits

$$|\varphi^+\rangle = |\phi_m^+\rangle^{\otimes m}, \quad |\varphi^-\rangle = |\phi_m^-\rangle^{\otimes m}. \quad (65)$$

Then, $\text{span}_{\mathbb{C}}\{|\varphi^+\rangle, |\varphi^-\rangle\}$ is a quantum error correction code with distance $d = m$. The proof is given in Appendix A. The reader might recognize that when $m = 3$, the code $\text{span}_{\mathbb{C}}\{|\varphi^+\rangle, |\varphi^-\rangle\}$ is nothing but Shor’s celebrated nine-qubit (repetition) code [42, 43]. The decomposition of the toric graph thus reveals an intriguing and apparently novel connection between the toric code and the repetition code.

The close connection between multiple GHZ states and the toric code is perhaps surprising. On the one hand, the GHZ states represent the long-range entanglement exhibited by topological states, spanning the length of the system. On the other hand, GHZ states are the most fragile many-qubit entangled states; a single measurement of any of the constituent qubits deletes all of the edges within the star graph. From Fig. 3, this corresponds to eliminating all qubits from a given row or column. Because of the translational invariance, however, the resulting toric graph maintains the same connectivity on the remaining qubits. Thus, the toric graph is effectively invariant under single-qubit measurements, demonstrating the robustness of the underlying topology.

Moreover, the multi-copy GHZ state is also a simple example of the distance balancing technique proposed in Ref. [44]. Consider the code $\text{span}_{\mathbb{C}}\{|\phi_m^+\rangle, |\phi_m^-\rangle\}$, in which $d_X = m$ and $d_Z = 1$, where d_X and d_Z are the distances with respect to X and Z errors, respectively. The distance balance method takes d_X/d_Z copies of such a code and outputs a new code with distance $\tilde{d}_X = \tilde{d}_Z = d_X$, at the cost of increasing the number of physical qubits. By adding another layer of structure corresponding to the half graphs, the degree of many vertices is not still bounded, yet the weight of the original stabilizer generators in the original (toric) code remains constant. The star graphs and half graphs thus play different key roles: the multi-star graphs contribute the large code distance while the half graphs ensure local stabilizer generators.

There is also a close resemblance between the code $\text{span}_{\mathbb{C}}\{|\varphi^+\rangle, |\varphi^-\rangle\}$ and the recently proposed repetition cat code [45] in the continuous variable setting, where two approximately orthogonal coherent states are used as the qubit registers $|0\rangle_c = |+\alpha\rangle$ and $|1\rangle_c = |-\alpha\rangle$. Similar to $\text{span}_{\mathbb{C}}\{|\phi_m^+\rangle, |\phi_m^-\rangle\}$, the bit flip error is exponentially suppressed ($d_X = m$) while the phase error is likely to occur ($d_Z = 1$). One therefore defines the repetition cat qubit state as $|\pm\rangle_L = |\pm\rangle_c^{\otimes r}$ in order to correct the phase error, which corresponds to $\text{span}_{\mathbb{C}}\{|\varphi^+\rangle, |\varphi^-\rangle\}$ if $r = m$.

IV. TORIC GRAPH STATE GENERATION

This section focuses on how to generate the toric code state within the quantum circuit model, in log depth in the absence of ancillae, and in constant depth including ancillae. The key step is to construct log-depth quantum circuits that generate the two toric code subgraphs: the star and half graphs.

The goal is to prepare the quantum state

$$|f\rangle = \frac{1}{\sqrt{2^N}} \sum_{q \in \{0,1\}^N} (-1)^{f(q)} |q\rangle \quad (66)$$

where the Boolean function $f : \{0,1\}^N \rightarrow \{0,1\}$ is associated with the binary quadratic form for a graph, Eq. (4). Given an operator U_f , which implements

$$U_f |q\rangle = (-1)^{f(q)} |q\rangle, \quad \forall q \in \{0,1\}^N, \quad (67)$$

one has $|f\rangle = U_f H^{\otimes N} |0^N\rangle$. Moreover, if f can be decomposed into the sum (module 2) of other Boolean functions, i.e. $f(q) = f_1(q) + \dots + f_k(q)$, then $|f\rangle$ can be generated by applying the commuting U_{f_i} operators in sequence:

$$|G\rangle = U_f^{(k)} \dots U_f^{(1)} H^{\otimes N} |0^N\rangle. \quad (68)$$

The target is the toric graph state

$$|G_{\text{toric}}\rangle = \frac{1}{\sqrt{2^{2L^2}}} \sum_{q \in \{0,1\}^{2L^2}} (-1)^{f_{\text{toric}}(q)} |q\rangle, \quad (69)$$

where $f_{\text{toric}}(q) = \sum_{n_1 < n_2} q_{n_1} q_{n_2} (A_{\text{toric}})_{n_1, n_2}$ is the quadratic Boolean form related to toric graph and

$$(A_{\text{toric}})_{n_1, n_2} = (A_{\text{toric}})_{i_1 j_1 d_1, i_2 j_2 d_2} \quad (70)$$

are the matrix elements of the graph adjacency matrix, Eq. (56). The variables $n_1, n_2 \in \{1, \dots, 2L^2\}$ are mapped to the qubit lattice coordinates ijd via

$$(i, j, d) \leftrightarrow i + (j-1)L + \delta_{dy} L^2. \quad (71)$$

Based on the decomposition of the toric graph and the relation between quadratic Boolean forms and the graph adjacency matrices, f_{toric} can be decomposed into

$$\begin{aligned} f_{\text{toric}} &= f_{\text{mstar}} + f_{\text{mhalf1}} + f_{\text{mhalf2}} \\ &= \sum_{jd} f_{jd}^{\text{star}} + \sum_j f_j^{\text{half1}} + \sum_j f_j^{\text{half2}}, \end{aligned} \quad (72)$$

where the adjacency matrices for f_{jd}^{star} , f_j^{half1} , and f_j^{half2} are defined in Eqs. (61) and (62), respectively. Thus, $|G_{\text{toric}}\rangle$ can be generated by the following circuits

$$|G_{\text{toric}}\rangle = \prod_j U_{f,j}^{\text{half2}} \prod_j U_{f,j}^{\text{half1}} \prod_{jd} U_{f,jd}^{\text{star}} H^{\otimes 2L^2} |0\rangle^{\otimes 2L^2}. \quad (73)$$

Different $U_{f,jd}^{\text{star}}$ operators have the same circuit depth, as they all compute the same quadratic Boolean function associated with an L -vertex star graph; moreover, each acts on different subsets of qubits, so all can be performed in parallel. The situation is similar for $U_{f,j}^{\text{half1}}$ and $U_{f,j}^{\text{half2}}$. To summarize: the depth of the toric code quantum circuit in Eq. (73) corresponds to the sum of the circuit depths for $U_{f,1x}^{\text{star}}$, $U_{f,1}^{\text{half1}}$ and $U_{f,1}^{\text{half2}}$.

A. Generation of the star graph state

The f_{jd}^{star} corresponds to the quadratic form for each L -vertex star graph, which is generically expressed as $f(q) = (q_1 + \dots + q_{c-1} + q_{c+1} + \dots + q_L) q_c$ with c labeling the high-degree central vertex, the value of which is unimportant. The term in parentheses corresponds to the parity $\text{Parity}(q_1, \dots, q_n)$ of an n -length string $q_1 \oplus \dots \oplus q_n$. The log-depth quantum circuit is inspired by the classical parity algorithm in a parallel setting. First, divide all n elements into $n/2$ disjoint pairs and calculate the parity of each subset in parallel; then continue subdividing until only one pair remains. It requires $\log_2 n$ iterations to obtain the parity of the bitstring (this of course ignores the n bits of classical communication required). In the quantum setting, the parity doesn't need to be calculated; only the two-qubit gates need to be implemented that generate the appropriate contribution to the Boolean function. The operations at each iteration commute, and therefore they can be truly implemented in parallel.

Without loss the generality, suppose the central vertex is the last one, and the unitary operation implementing Eq. (67) with $f(q) = (q_1 + \dots + q_{L-1}) q_L$ is

$$U_f^{\text{star}} = P^{-1} \text{CZ}(q_{L-1}, q_L) P, \quad (74)$$

in which P is a quantum operation that generates the parity linear form:

$$P |q\rangle = |q'\rangle, \quad (75)$$

where $q'_{L-1} = q_1 + \dots + q_{L-1}$. The operator P can be implemented using a series of CX = CNOT gates, which have the action

$$\text{CX}(1, 2) |q_1, q_2\rangle = |q_1, q_1 + q_2\rangle. \quad (76)$$

One first divides the first $L-1$ qubits into $(L-1)/2$ disjoint pairs and calculates the parity of each pair in parallel:

$$\prod_{i=1}^{\lfloor (L-1)/2 \rfloor} \text{CX}(2i-1, 2i) |q\rangle = |\tilde{q}\rangle, \quad (77)$$

where $|\tilde{q}\rangle$ denotes the state in quantum register after first iteration and $\tilde{q}_{2i} = q_{2i-1} + q_{2i}$. If $L-1$ is odd, then the $L-1$ -th qubit does not need to be explicitly paired. One then divides the $\lceil \frac{L-1}{2} \rceil$ quantum registers with the parity

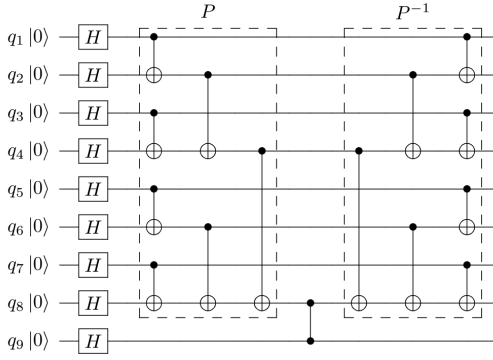


FIG. 5. Quantum circuit that generates a nine-qubit star graph state

result to $(L-1)/4$ pairs, and repeats the procedure until all of the clauses have been paired. After $\log(L-1)$ iterations, one obtains the result in the $L-1$ -th register as $q'_{L-1} = q_1 + \dots + q_{L-1}$. Next, the CZ gate implements the required phase:

$$\begin{aligned} \text{CZ}(L-1, L) |q'\rangle &= (-1)^{q'_{L-1} \cdot q'_L} |q'\rangle \\ &= (-1)^{(q_1 + \dots + q_{L-1}) q_L} |q'\rangle. \end{aligned} \quad (78)$$

As U_f^{star} should yield $(-1)^{f(q)} |q\rangle$ as the output state, one must implement the inverse of P to change $|q'\rangle$ to $|q\rangle$:

$$P^{-1}(-1)^{f(q)} |q'\rangle = (-1)^{f(q)} |q\rangle. \quad (79)$$

The nine-qubit example for U_f^{star} is shown in Fig. 5. The construction of P for arbitrary number of qubits, Algorithm 1, and the proof of its log depth are given in Appendix B. Thus, the depth of $U_{f,1x}^{\text{star}}$ is $O(\log L)$. Note that a log-depth circuit for the realization of GHZ states has been obtained recently by other means [46].

B. Generation of the half graph state

The Boolean quadratic forms f_j^{half1} and f_j^{half2} are associated with the $2(L-1)$ -vertex half graph, so the current task is to construct a quantum circuit that computes f_h . For a $2n$ -vertex half graph, $f_h(q, p) = \sum_{i \leq j} q_i p_j$, where $i, j \in \{1, \dots, n\}$. Moreover, $f_h(q, p)$ can be decomposed in the following way:

$$f_h(q, p) = \sum_{k=0}^{\lceil \log n \rceil} f_h^{(k)}(q, p), \quad (80)$$

where

$$\begin{aligned} f_h^{(k)}(q, p) &= \sum_{i=0}^{n/2^k - 1} \left(\sum_{j=2^k i + 1}^{2^k(i + \frac{1}{2})} q_j \right) \left(\sum_{j=2^k(i + \frac{3}{2})}^{2^k(i + 1)} p_j \right) \end{aligned} \quad (81)$$

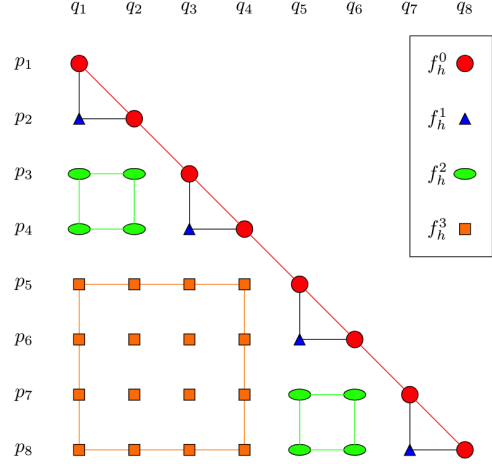


FIG. 6. (Color online) Decomposition of $f_h(q, p)$ when $n = 2^3$.

assuming that n is a power of two. Otherwise, one need only replace the sum upper bound by $n/2^k \rightarrow \lceil n/2^k \rceil$, $2^k(i + 1/2) \rightarrow \min\{2^k(i + 1/2), n\}$, and $2^k(i + 1) \rightarrow \min\{2^k(i + 1), n\}$. For simplicity of analysis one can assume that n is a power of two, but the results hold for arbitrary integer values. A few decomposed Boolean functions are listed as follows:

$$\begin{aligned} f_h^{(0)}(q, p) &= \sum_{i=0}^{n-1} q_{i+1} p_{i+1}; \\ f_h^{(1)}(q, p) &= \sum_{i=0}^{n/2-1} q_{2i+1} p_{2i+2}; \\ f_h^{(2)}(q, p) &= \sum_{i=0}^{n/4-1} (q_{4i+1} + q_{4i+2})(p_{4i+3} + p_{4i+4}); \\ f_h^{(\log_2 n)}(q, p) &= \left(\sum_{j=1}^{n/2} q_j \right) \left(\sum_{j=n/2+1}^n p_j \right), \end{aligned} \quad (82)$$

The decomposition for $f_h(q, p)$ when $n = 2^3$ is shown in Fig 6, from which one may obtain an intuition of why the decomposition Eq. (80) holds in general. In Fig 6, the columns correspond to variable q_i and the rows correspond to variable p_i . Each element represents a term $q_i p_j$ appearing in $f_h(q, p)$. From the condition $i \leq j$ in the sum of $f_h(q, p)$, one obtains the representation as a triangle. The decomposition Eq. (80) corresponds to separating the triangle into a square and two triangles of half size iteratively. For example, the $2^3 \times 2^3$ triangle in Fig 6 is decomposed into the left bottom $2^2 \times 2^2$ square (corresponding to $f_h^{(3)}$) and two $2^2 \times 2^2$ triangles above and on the right of it. Decomposing these triangles in turn yields 2×2 square (corresponding to the $f_h^{(2)}$), with the $f_h^{(1)}$ and $f_h^{(0)}$ terms remaining.

Each square corresponds to a term in the Boolean function of the form $(\sum_i q_i)(\sum_j p_j)$, where $(\sum_i q_i)$ again cor-

responds to the parity operation which can be implemented in log depth. The sum in Eq. (81) consists of $n/2^k$ squares of side length 2^{k-1} . As different squares associated to the same k share no common variables, their parity operations can be implemented in parallel. Combining Eqs. (68) and (80), the half graph operators can therefore be implemented with a $O(\log^2 n)$ -depth quantum circuit.

This circuit depth can be further reduced by a more careful construction. Note that one of the sums in the penultimate term of Eq. (80)

$$f_h^{(\log_2 n - 1)}(q, p) = \left(\sum_{j=1}^{n/4} q_j \right) \left(\sum_{j=n/4+1}^{n/2} p_j \right) + \left(\sum_{j=n/2+1}^{3n/4} q_j \right) \left(\sum_{j=3n/4+1}^n p_j \right), \quad (83)$$

already includes half of the terms required by the final term $f_h^{(\log_2 n)}(q, p)$. Thus, if one were to also include the calculation of $\sum_{j=1+n/4}^{n/2} q_j$ and $\sum_{j=n/2+1}^{3n/4} p_j$ at level $\log_2 n - 1$ (which shares no variables with other terms at this level), the level- $\log_2 n$ calculation would require only $O(1)$ operations (one multiplication). Applying this idea recursively, we can compute f_h using a $O(\log n)$ -depth quantum circuit, so the depth of f_{half1} and f_{half2} are both $O(\log L)$.

Let's consider each term more carefully. The $f_h^{(0)}$ term is the sum of multiplications, all of which share no common variables, so that $U_{f_h^{(0)}}$ can be implemented as a depth-one quantum circuit:

$$U_{f_h^{(0)}} |q, p\rangle = \prod_{i=1}^n \text{CZ}(q_i, p_i) |q, p\rangle = (-1)^{f_h^{(0)}(q, p)} |q, p\rangle. \quad (84)$$

Similarly,

$$U_{f_h^{(1)}} |q, p\rangle = \prod_{i=0}^{n/2-1} \text{CZ}(q_{2i+1}, p_{2i+2}) |q, p\rangle = (-1)^{f_h^{(1)}(q, p)} |q, p\rangle, \quad (85)$$

is also obtained with a depth-one quantum circuit. To construct $U_{f_h^{(2)}}$, one requires CX gates because the sum term involves the parity of two bits:

$$\begin{aligned} |q^{(2)}, p^{(2)}\rangle &= \prod_i^{n/4-1} \text{CX}(q_{4i+1}, q_{4i+2}) \text{CX}(q_{4i+3}, q_{4i+4}) \\ &\quad \times \text{CX}(p_{4i+1}, p_{4i+2}) \text{CX}(p_{4i+3}, p_{4i+4}) |p, q\rangle, \end{aligned} \quad (86)$$

where

$$\begin{aligned} q_{4i+2}^{(2)} &= q_{4i+1} + q_{4i+2}, & q_{4i+4}^{(2)} &= q_{4i+3} + q_{4i+4}, \\ p_{4i+2}^{(2)} &= p_{4i+1} + p_{4i+2}, & p_{4i+4}^{(2)} &= p_{4i+3} + p_{4i+4}. \end{aligned} \quad (87)$$

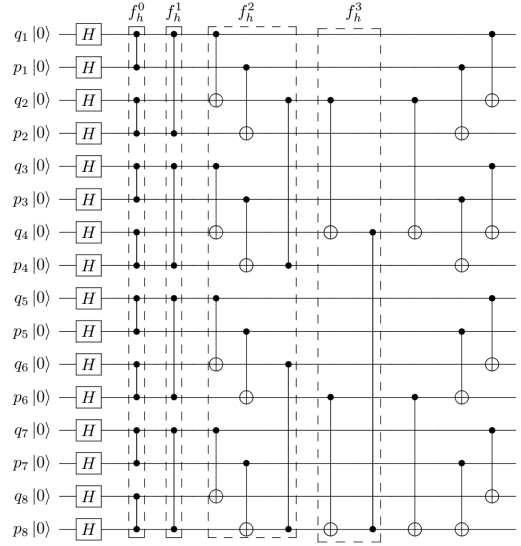


FIG. 7. Quantum circuit that generates a 16-qubit half graph state

The CZ operation then yields the desired phase:

$$\begin{aligned} &\prod_{i=0}^{n/4-1} \text{CZ}(q_{4i+2}, q_{4i+4}) |q^{(2)}, p^{(2)}\rangle \\ &= (-1)^{\sum_{i=0}^{n/4-1} q_{4i+2}^{(2)} \cdot p_{4i+4}^{(2)}} |q^{(2)}, p^{(2)}\rangle \\ &= (-1)^{f_h^{(2)}(q, p)} |q^{(2)}, p^{(2)}\rangle. \end{aligned} \quad (88)$$

As the parity operator needs to also be used in the next iteration, the inverse of Eq. (86) is not applied immediately, but rather only after all the phases $(-1)^{f_h^{(k)}(q, p)}$ have been added. Eqs. (86) and (88) correspond to a depth-two quantum circuit which implements a phase $(-1)^{f_h^{(2)}(q, p)}$, and the same is true for all $k > 2$. After the $\log(n)$ iteration, one obtains $(-1)^{f_h(q, p)} |q', p'\rangle$ by means of a quantum circuit of total depth $2 \log(n)$. One then applies the inverse of all the CX gates so that the state in the quantum register is changed to $(-1)^{f_h(q, p)} |q, p\rangle$, so U_{f_h} is implemented using a $3 \log(n)$ -depth quantum circuit.

The explicit circuit for the 16-qubit example is shown in Fig. 7. The generic algorithm for arbitrary numbers of qubits, Algorithm 2, and the proof of its log depth, are included in Appendix C. Thus, one can generate $|G_{\text{toric}}\rangle$ via Eq. (73) in log depth.

C. Reduction to constant depth

Any graph can be expanded to a graph containing vertices with at most degree three, by introducing ancillae [40] which are then measured in the X basis. Given that all the measurements commute and can therefore be performed simultaneously, graph state preparation can

be performed in (constant) depth three. For example, the star graphs on L qubits with degree $L - 1$ that are induced subgraphs of the toric graph can be represented by a totally asymmetric tree graph with $2L - 4$ vertices with maximum degree three. Given that there are $2L$ star graphs comprising the toric graph, the contribution of the star-graph ancillae to the circuit width scales as $L^2 \sim N$.

Next consider the half graphs on $2(L - 1)$ vertices that constitute the remaining subgraphs. The first vertex in the first of the two bipartite vertex subsets has an edge with all $L - 1$ vertices in the second vertex subset and thus has the connectivity of a degree- $L - 1$ star graph; following the procedure described for the star graphs, one can add $L - 4$ ancillae to this central vertex to ensure that all resulting vertices have at most degree three. The second vertex in the first subset shares $L - 2$ neighbors in the second subset, requiring the addition of $L - 5$ ancillae, etc. The total number of required ancillae therefore scales as L^2 ; and, given that the number of half graphs scales as L , the total number of half-graph ancillae scales as L^3 . Thus, preparing the toric graph of size N in constant depth as a maximum degree-three graph requires a circuit width $\mathcal{O}(L^3) \sim \mathcal{O}(N^{3/2})$.

It is worthwhile to point out that the $\mathcal{O}(L^3)$ -qubit graph state with bounded degree-three vertices is topologically trivial, while the state that remains after the X measurements is the topologically ordered toric graph state. Thus, one can obtain a topologically ordered state by projective measurement on a topologically trivial state in a higher-dimensional Hilbert space.

V. DISCUSSION

In this work, we provide an explicit quantum circuit which generates the toric code states on N qubits in $\log(N)$ depth, or in constant depth if the circuit width is allowed to increase as $N^{3/2}$, under the assumption of geometrically non-local gates. By using the local-Clifford equivalence of stabilizer and graph states, the toric code state generation is first reduced to preparing the toric graph state, which is found to consist solely of star and half graphs. The quantum circuit is then obtained as an efficient set of gates that effects the quadratic Boolean function associated with the graph adjacency matrix.

Given that the star graphs encode GHZ states, the graph construction reveals a novel connection between the toric code and the nine-qubit (repetition) error correcting code, which is itself an instance of a family of codes with macroscopic code distance. The star graphs therefore contribute the large code distance, while the half graphs ensure that the toric code stabilizer generators are low-weight and geometrically local. The graph state connectivity also explicitly reveals the long-range entanglement exhibited by the toric code states, and provides direct insight into the robustness of the state against the loss of physical qubits.

These results provide a method to generate any 2D topological stabilizer state with translation symmetry. It was shown in Ref. [17] not only that all 2D translationally invariant topological stabilizer codes are in the same universal phase, but also that they can all be mapped to multiple copies of the toric code. As quantum states in the same topological phase can be transformed to each other through a constant-depth quantum circuit [18], all 2D topological stabilizer code states with translation symmetry can be generated using a log-depth quantum circuit via our method.

A fruitful avenue for future research would be to probe what features of the toric graph are specific to the toric code, and what features (if any) are necessary to ensure that the graph connectivity encodes a state with non-trivial topological order. For example, the multiple copies of the star graph are sufficient to ensure that the code distance increases polynomially with the number of physical qubits. Presumably other subgraphs could accomplish the same, but potentially at the cost of increasing the minimum weight of the associated stabilizer generators. In any case, constructing the graph state first and then reversing the mapping to the stabilizer set could allow for the discovery of new classes of topological error-correction codes.

ACKNOWLEDGMENTS

The authors are grateful to Barry Sanders for insightful comments. This work was supported by the Natural Sciences and Engineering Research Council of Canada.

Appendix A: Multiple copies of the GHZ state

Remark. Given two m -qubit GHZ states

$$|\phi_m^+\rangle = \frac{|0^m\rangle + |1^m\rangle}{\sqrt{2}}, \quad |\phi_m^-\rangle = \frac{|0^m\rangle - |1^m\rangle}{\sqrt{2}}. \quad (\text{A1})$$

and their m -copy states on m^2 qubits

$$|\varphi^+\rangle = |\phi_m^+\rangle^{\otimes m}, \quad |\varphi^-\rangle = |\phi_m^-\rangle^{\otimes m}. \quad (\text{A2})$$

Then, $\text{span}_{\mathbb{C}} \{ |\varphi^+\rangle, |\varphi^-\rangle \}$ is a quantum error correction code with distance $d = m$.

Proof. The weight of the operator $O \in \mathcal{P}_N$ is the number of qubits which are acted on non-trivially (i.e. by a non-identity) by O . Here, $\mathcal{P}_N^d \subset \mathcal{P}_N$ contains all the operators whose weight is less than d . Based on the quantum error correction condition [43, 47], the subspace $\text{span}_{\mathbb{C}} \{ |\psi_1\rangle, |\psi_2\rangle \} \subset \mathcal{H}_2^{\otimes N}$ is a quantum error correction code with distance d if and only if the following conditions always hold:

$$\langle \psi_1 | O | \psi_1 \rangle = \langle \psi_2 | O | \psi_2 \rangle, \quad (\text{A3})$$

$$\langle \psi_1 | O | \psi_2 \rangle = 0, \quad (\text{A4})$$

Algorithm 1 Generate star graph state

Require:

unsignedinteger NUM

▷ number of qubits

Ensure:

binary[NUM] QSTATE

▷ NUM-qubit star graph state

1: **function** GENERATE STAR GRAPH STATE(NUM)

2: unsignedinteger DEPTH

▷ Depth of the circuit

3: unsignedinteger QTARG

▷ Index of target qubit

4: QSTATE $\leftarrow 0^{\text{NUM}}$

▷ Initialize quantum register

5: QSTATE $\leftarrow H[\text{NUM}] \cdot \text{QSTATE}$

▷ Apply Hadamard gate

6: DEPTH $\leftarrow \lceil \log(\text{NUM} - 1) \rceil$ 7: **for** d from 1 to in DEPTH **do**8: **for** i from 2^{d-1} to NUM-1 **do**9: **if** $i = 2^{d-1} \bmod 2^d$ **then**10: QTARG $\leftarrow \min\{i + 2^{d-1}, \text{NUM} - 1\}$ 11: QSTATE $\leftarrow CX(i, \text{QTARG}) \cdot \text{QSTATE}$

▷ Apply CX gate

12: **end if**13: **end for**14: **end for**15: QSTATE $\leftarrow CZ(\text{NUM} - 1, \text{NUM}) \cdot \text{QSTATE}$

▷ Apply CZ gate

16: **for** d from DEPTH to 1 **do**17: **for** i from 2^{d-1} to NUM **do**18: **if** $i - 2^{d-1} = 0 \bmod 2^d$ **then**19: QTARG $\leftarrow \min\{i + 2^{d-1}, \text{NUM} - 1\}$ 20: QSTATE $\leftarrow CX(i, \text{QTARG}) \cdot \text{QSTATE}$ 21: **end if**22: **end for**23: **end for**24: **end function**

for every operator $O \in \mathcal{P}_N^d$.

It is straightforward to verify that $\langle \phi_m^+ | O | \phi_m^+ \rangle = \langle \phi_m^- | O | \phi_m^- \rangle$ is satisfied $\forall O \in \mathcal{P}_m^m$, while the second condition fails to hold because $\langle \phi_m^+ | Z_i | \phi_m^- \rangle = 1$, where Z_i is the Pauli Z operator acting on qubit i . Consider multiple copies of the GHZ state instead. One can again verify that $\langle \varphi^+ | O | \varphi^+ \rangle = \langle \varphi^- | O | \varphi^- \rangle$ still holds $\forall O \in \mathcal{P}_m^m$. On the other hand, one obtains

$$\langle \varphi^+ | O | \varphi^- \rangle = \langle \varphi^+ | \bigotimes_{i=1}^m O_i | \varphi^- \rangle = \prod_{i=1}^m \langle \phi_m^+ | O_i | \phi_m^- \rangle, \quad (\text{A5})$$

where $O_i \in \mathcal{P}_m$ acts on the i -th copy. If $\langle \varphi^+ | O | \varphi^- \rangle \neq 0$, then $\langle \phi_m^+ | O_i | \phi_m^- \rangle \neq 0, \forall i \in \{1, \dots, m\}$, so O acts on at least m qubits non-trivially and $O \notin \mathcal{P}_m^m$. Therefore,

condition Eq. (A3) and Eq. (A4) hold $\forall O \in \mathcal{P}_m^m$ for $|\varphi^+\rangle$ and $|\varphi^-\rangle$. \square

Appendix B: Quantum circuit generating star graph states

In this section, we prove that Algorithm 1 generates a star graph state in log depth. Line 1 to line 5 describe the initialization process and the state in quantum register after line 5 is $H^{\otimes n} |0^n\rangle$. Next, the circuit described from line 6 to line 14 is the gate P in Eq. (74) that implement $\text{Parity}(q_1, \dots, q_{n-1})$. Line 15 adds a global phase $(-1)^{\text{Parity}(q_1, \dots, q_{n-1}) \cdot q_n}$ and the remaining operation is exactly inverse of P . It only remains to prove that line 6 to line 14 indeed implements $\text{Parity}(q_1, \dots, q_{n-1})$.

Consider the action from line 6 to line 14 on input $|q\rangle$, a computational basis state and $q \in \{0, 1\}^n$. d denotes the times of iteration and $|q^d\rangle$ is the state in quantum register after the d -th iteration. During the d -th iteration, the gate $CX(2^{d-1} + c2^d, (c+1)2^d)$, where $c \in \mathbb{N}$, is executed. One notices that all CX gates within the same iteration act on no common qubits so they can all be performed in parallel. The depth of the circuit from line 6 to line 14 is then $\log(n-1)$.

After d -th iteration, the state in the quantum register should satisfy $q_{c2^d}^d = \sum_{j=(c-1)2^{d+1}}^{c2^d} q_j$, where $c \in \{1, \dots, 2^{\lceil \log(n-1) \rceil - d}\}$. We prove this claim using induction. First, it holds trivially when $d = 0$. Next, suppose it holds when $d = k$. Then in the $(k+1)$ -th loop, gate $CX(c2^{k+1} - 2^k, c2^{k+1})$ is executed, where

Algorithm 2 Generate half graph state

Require:
 unsignedinteger NUM ▷ size of the half graph

Ensure:
 binary[2NUM] QSTATE ▷ 2NUM-qubit half graph state

```

1: function GENERATE HALF(NUM)
2:   unsignedinteger DEPTH ▷ Depth of the circuit
3:   unsignedinteger CONXQBIT
4:   unsignedinteger CONYQBIT
5:   unsignedinteger TARXQBIT
6:   unsignedinteger TARYQBIT
7:   QSTATEx ← 0NUM ▷ Quantum register for |q⟩
8:   QSTATEx ← HAD(NUM) * QSTATEx
9:   QSTATEY ← 0NUM ▷ Quantum register for |p⟩
10:  QSTATEY ← HAD(NUM) * QSTATEY
11:  for i from 1 to NUM do
12:    CONXQBIT ← i
13:    TARYQBIT ← i
14:    QSTATE ← CZ(CONXQBIT, TARYQBIT) * (QSTATEx, QSTATEY)
15:  end for
16:  DEPTH ← ⌈log(NUM)⌉
17:  for d from 1 to in DEPTH do
18:    for i from 1 to NUM do
19:      if i = 2d-1 mod 2d then
20:        CONXQBIT ← i
21:        CONYQBIT ← i
22:        TARXQBIT ← min{i + 2d-1, NUM}
23:        TARYQBIT ← min{i + 2d-1, NUM}
24:        QSTATE ← CZ(CONXQBIT, TARYQBIT) * (QSTATEx, QSTATEY)
25:        QSTATEx ← CX(CONXQBIT, TARXQBIT) * QSTATEx
26:        QSTATEY ← CX(CONYQBIT, TARYQBIT) * QSTATEY
27:      end if
28:    end for
29:  end for
30:  for d from DEPTH to 1 do
31:    for i from 2d-1 to NUM do
32:      if i - 2d-1 = 0 mod 2d then
33:        CONXQBIT ← i
34:        CONYQBIT ← i
35:        TARXQBIT ← min{i + 2d-1, NUM}
36:        TARYQBIT ← min{i + 2d-1, NUM}
37:        QSTATEx ← CX(CONXQBIT, TARXQBIT) * QSTATEx
38:        QSTATEY ← CX(CONYQBIT, TARYQBIT) * QSTATEY
39:      end if
40:    end for
41:  end for
42: end function

```

$c \in \{1, \dots, 2^{\lceil \log(n-1) \rceil - k - 1}\}$, so

$$\begin{aligned}
q_{c2^{k+1}}^{k+1} &= q_{c2^{k+1}}^k + q_{c2^{k+1}-2^k}^k = q_{2c2^k}^k + q_{(2c-1)2^k}^k \\
&= \sum_{j=(2c-1)2^k+1}^{2c2^k} q_j + \sum_{j=(2c-2)2^k+1}^{(2c-1)2^k} q_j \\
&= \sum_{j=(c-1)2^{k+1}+1}^{c2^{k+1}} q_j.
\end{aligned} \tag{B1}$$

If $\log_2(n-1) \in \mathbb{N}$, then after $\log_2(n-1)$ -th iteration, $q_{n-1}^{\log_2(n-1)} = \text{Parity}(q_1, \dots, q_{n-1})$. When $\log_2(n-1) \notin \mathbb{N}$,

then in the $\log_2(n-1)$ -th iteration, the target qubit is replace as $n-1$ -th qubit when it exceed $n-1$ in line 10, so $q_{n-1}^{\lceil \log_2(n-1) \rceil} = \text{Parity}(q_1, \dots, q_{n-1})$ still holds. Therefore, we conclude Algorithm 1 indeed generates a star graph state in log depth.

Appendix C: Quantum circuit generating half states

The Unitary described from line 11 to line 15 adds the phase $(-1)^{f_h^k(q,p)}$. Next, consider what unitary lines 16-

29 computes when the input is in the computational basis $|q, p\rangle$. $|q^d, p^d\rangle$ denotes the state in the register after the d -th iteration. The operation within the quantum register for $|q\rangle$ ($|p\rangle$) is the same as in Algorithm 1, so after $k-1$ -th iteration

$$q_{c2^{k-1}}^{k-1} = \sum_{j=(c-1)2^{k-1}+1}^{c2^{k-1}} q_j, \quad (C1)$$

$$p_{c2^{k-1}}^{k-1} = \sum_{j=(c-1)2^{k-1}+1}^{c2^{k-1}} p_j, \quad (C2)$$

holds. In addition, in the k -th iteration, gate $\text{CZ}(q_{c2^k-2^{k-1}}, p_{c2^k})$ is executed with the quantum register in state $|q^{k-1}, p^{k-1}\rangle$, adding a phase $(-1)^{f'_k(q,p)}$,

where

$$\begin{aligned} f'_k(q, p) &= \sum_{c=1}^{n/2^k} q_{c2^k-2^{k-1}}^{k-1} \cdot p_{c2^k}^{k-1} \\ &= \sum_{c=1}^{n/2^k} \left(\sum_{j=(2c-2)2^{k-1}+1}^{(2c-1)2^{k-1}} q_j \right) \cdot \left(\sum_{j=(2c-1)2^{k-1}+1}^{2c2^{k-1}} p_j \right) \\ &= \sum_{c=0}^{n/2^k-1} \left(\sum_{j=c2^k+1}^{(c+1/2)2^k} q_j \right) \cdot \left(\sum_{j=(c+1/2)2^k+1}^{(c+1)2^k} p_j \right) \\ &= f_h^k(q, p). \end{aligned} \quad (C3)$$

When n is not the power of two, the sum index upper bound is replaced in line 22 and line 23. Therefore, the quantum circuit in the k -th iteration adds a global phase $(-1)^{f_h^k(q,p)}$ and all CZ (CX) gates within the same iteration can be performed in parallel. Lines 30-41 uncompute the garbage and leave only the phase. Because of the decomposition Eq. (80), this algorithm prepares a half graph state in log depth.

-
- [1] A. Y. Kitaev, in *Proceedings of the Third International Conference on Quantum Communication and Measurement*, edited by O. Hirota, A. S. Holevo, and C. M. Caves (Plenum, 1997).
 - [2] A. Y. Kitaev, *Fault-tolerant quantum computation by anyons* (1997), arXiv:quant-ph/9707021.
 - [3] A. Y. Kitaev, *Annals of Physics* **303**, 2 (2003).
 - [4] C. Nayak, S. H. Simon, A. Stern, M. Freedman, and S. Das Sarma, *Rev. Mod. Phys.* **80**, 1083 (2008).
 - [5] A. Stern and N. H. Lindner, *Science* **339**, 1179 (2013), ISSN 0036-8075.
 - [6] V. Lahtinen and J. K. Pachos, *SciPost Phys.* **3**, 021 (2017).
 - [7] E. Dennis, A. Kitaev, A. Landahl, and J. Preskill, *Journal of Mathematical Physics* **43**, 4452 (2002).
 - [8] M. A. Levin and X.-G. Wen, *Phys. Rev. B* **71**, 045110 (2005).
 - [9] H. Bombin and M. A. Martin-Delgado, *Phys. Rev. Lett.* **97**, 180501 (2006).
 - [10] Y. Xia, D. Qian, D. Hsieh, L. Wray, A. Pal, H. Lin, A. Bansil, D. Grauer, Y. S. Hor, R. J. Cava, et al., *Nature Physics* **5**, 398 (2009), ISSN 1745-2481.
 - [11] S. M. Albrecht, A. P. Higginbotham, M. Madsen, F. Kuemmeth, T. S. Jespersen, J. Nygård, P. Krogstrup, and C. M. Marcus, *Nature* **531**, 206 (2016).
 - [12] R. S. K. Mong, D. J. Clarke, J. Alicea, N. H. Lindner, P. Fendley, C. Nayak, Y. Oreg, A. Stern, E. Berg, K. Shtengel, et al., *Phys. Rev. X* **4**, 011036 (2014).
 - [13] C. V. Kraus, P. Zoller, and M. A. Baranov, *Phys. Rev. Lett.* **111**, 203001 (2013).
 - [14] J. D. Sau, R. M. Lutchyn, S. Tewari, and S. Das Sarma, *Phys. Rev. Lett.* **104**, 040502 (2010).
 - [15] J. Alicea, Y. Oreg, G. Refael, F. von Oppen, and M. P. A. Fisher, *Nature Physics* **7**, 412 (2011), ISSN 1745-2481.
 - [16] D. Gottesman, *Stabilizer codes and quantum error correction* (1997), arXiv:quant-ph/9705052.
 - [17] H. Bombin, G. Duclos-Cianci, and D. Poulin, *New Journal of Physics* **14**, 073048 (2012), ISSN 1367-2630.
 - [18] X. Chen, Z.-C. Gu, and X.-G. Wen, *Phys. Rev. B* **82**, 155138 (2010).
 - [19] F. Liu, S. Whitsitt, J. B. Curtis, R. Lundgren, P. Titum, Z.-C. Yang, J. R. Garrison, and A. V. Gorshkov, *Phys. Rev. Research* **2**, 013323 (2020).
 - [20] S. Bravyi, M. B. Hastings, and F. Verstraete, *Phys. Rev. Lett.* **97**, 050401 (2006).
 - [21] A. Hamma and D. A. Lidar, *Phys. Rev. Lett.* **100**, 030502 (2008).
 - [22] D. Aharonov and A. Ta-Shma (Association for Computing Machinery, New York, NY, USA, 2003), STOC '03, pp. 20-29, ISBN 1581136749.
 - [23] Y. Huang and X. Chen, *Phys. Rev. B* **91**, 195143 (2015).
 - [24] A. Rahmani, K. J. Sung, H. Putterman, P. Roushan, P. Ghaemi, and Z. Jiang, *PRX Quantum* **1**, 020309 (2020).
 - [25] J. Eisert, K. Jacobs, P. Papadopoulos, and M. B. Plenio, *Phys. Rev. A* **62**, 052317 (2000).
 - [26] J. I. Cirac, W. Dür, B. Kraus, and M. Lewenstein, *Phys. Rev. Lett.* **86**, 544 (2001).
 - [27] L. Yu, R. B. Griffiths, and S. M. Cohen, *Phys. Rev. A* **81**, 062315 (2010).
 - [28] S. M. Cohen, *Phys. Rev. A* **81**, 062316 (2010).
 - [29] A. Soeda, P. S. Turner, and M. Mura, *Phys. Rev. Lett.* **107**, 180501 (2011).
 - [30] L. Yu, R. B. Griffiths, and S. M. Cohen, *Phys. Rev. A* **85**, 012304 (2012).
 - [31] N. Vyas, D. Saha, and P. K. Panigrahi, *Quantum Information Processing* **15**, 3855 (2016).
 - [32] P. K. Vishnu, D. Joy, B. K. Behera, and P. K. Panigrahi, *Quantum Information Processing* **17**, 274 (2018).

- [33] D. Aharonov and Y. Touati, *Quantum circuit depth lower bounds for homological codes* (2018), 1810.03912.
- [34] M. Aguado and G. Vidal, Phys. Rev. Lett. **100**, 070404 (2008).
- [35] D. Schlingemann, Quant. Inf. Comput. **2**, 307 (2002).
- [36] M. Van den Nest, J. Dehaene, and B. De Moor, Phys. Rev. A **69**, 022316 (2004).
- [37] M. Hein, J. Eisert, and H. J. Briegel, Phys. Rev. A **69**, 062311 (2004).
- [38] P. Erdős, in *Measure Theory Oberwolfach 1983*, edited by D. Kölzow and D. Maharam-Stone (Springer Berlin Heidelberg, Berlin, Heidelberg, 1984), pp. 321–327.
- [39] A. Cosentino and S. Severini, Phys. Rev. A **80**, 052309 (2009).
- [40] P. Høyer, M. Mhalla, and S. Perdrix, in *17th International Symposium on Algorithms and Computation* (2006), vol. 4288, pp. 638–649.
- [41] J. Dehaene, M. Van den Nest, B. De Moor, and F. Verstraete, Phys. Rev. A **67**, 022310 (2003).
- [42] P. W. Shor, Phys. Rev. A **52**, R2493 (1995).
- [43] M. Nielsen and I. Chuang, *Quantum Computation and Quantum Information*, Cambridge Series on Information and the Natural Sciences (Cambridge University Press, 2000), ISBN 9780521635035.
- [44] M. B. Hastings, arXiv preprint arXiv:1611.03790 (2016).
- [45] J. Guillaud and M. Mirrahimi, Phys. Rev. X **9**, 041053 (2019).
- [46] D. Cruz, R. Fournier, F. Gremion, A. Jeannerot, K. Komagata, T. Tosić, J. Thiesbrummel, C. L. Chan, N. Macris, M.-A. Dupertuis, et al., Advanced Quantum Technologies **2**, 1900015 (2019).
- [47] E. Knill and R. Laflamme, Phys. Rev. A **55**, 900 (1997).